Jets and droplets compared to a moving slab of liquid for divertor cooling for a tokamak magnetic fusion energy reactor

Ralph W. Moir
Vallecitos Molten Salt Research
607 E. Vallecitos Rd.
Livermore, CA 94550
Rmoir@Pacbell.net 925-447-8804 phone/fax

March 17, 2008

Abstract

Moving liquid surfaces can be used to carry away heat from the exhaust plasma of a magnetic fusion reactor; however, these surfaces will warm up quickly and increase their evaporative flux. Any strategy that decreases the surface temperature rise will be effective in decreasing the evaporative flux, which is exponentially dependent on surface temperature. Jets and droplets are compared to a moving slab of the same liquid for a tokamak divertor as an example. The droplets are coherent in the sense that the droplets from different jets in the array are aligned and shadow each other. One figure of merit is the net evaporative flux averaged over the divertor surface compared to the flux of ions striking the surface. Contrary to some prior studies we find configurations of jets and droplets with lower evaporative flux than a moving slab of the same speed. Further more, droplets are strongly preferred because they are stable and can be produced at very high speeds whereas either a slab or jets will breakup owing to turbulence. Molten salts (flibe) at a speed of 40 m/s can handle about 25 MW/m^2 normal to the poloidal power flux and this is less power than liquid metals by about a factor of four for our tokamak example. If liquid walls are used, then the liquid for the divertor should be the same liquid as that of the liquid walls.

Table of contents

Notation list

Γ=power per unit area on the divertor
v=speed of injected liquid
t=time moving along injected liquid as it passes through the divertor
θ =angles defined in Fig. 5.
ϕ=angles defined in Fig. 5.
ψ=angles defined in Fig. 5.
ω=angles defined in Fig. 5.
p_z=spacing between layers of jets
p=p_z=spacing between jets
P/A=Γ
$(P/A)_{peak}$=Power per unit area normal to the plasma flow
f=frequency of acoustic pressure to produce precisely sized droplets
L=axial spacing of droplets
d_j=diameter of jets
d_d=diameter of droplet
σ=surface tension
Re=Reynolds number
Pr=Prandl number
We=Weber number
Ca=Capillary number
ρ=density of liquid
η=viscosity of liquid
v_s=surface speed of liquid circulation or spin
k=thermal conductivity of liquid
C=heat capacity of liquid
X_{th}=thermal diffusion distance
J=evaporative flux, #/m^2s
P=vapor pressure

Background

As background we know [based on calculations by Ulrickson (2000)] that liquid jets or droplets have a problem relative to a liquid slab in that the jet can have a high power per unit area due to the perpendicular power flux whereas a slab can have this power per unit area diminished by the sin of the angle between the incidence flux and the plane of the slab. In the tokamak example case the angle is only 2.58° (87.4° from the normal) and the incident power flux is diminished by a factor of 22. Evaporation depends exponentially on the surface temperature that in turn depends linearly on the incident power flux. Ulrickson reasoned that only a small deviation from this small angle would greatly increase the power density on the surface and hence its evaporation rate and surely perpendicular incidence on jets or droplets would result in a very large evaporative flux.

Further more there was a study of droplets versus slabs by Zhou and Tillack (1998) that found slab could handle 2.4 to 4 times the power density that the droplets could handle depending on their assumptions.

Droplets can be made of precise size and spatially coherent from one jet to the next so that they can shadow each other. This effect discussed later and shown in Fig. 4 forms the basis of this paper. We are interested in liquid divertors partly because with liquid walls the divertor will be liquid whether we want it or not. Therefore the divertor liquid should be the same liquid as the walls.

Introduction

In this work we will show that relatively closed packed jets or droplets can be self shielded so that the incoming power is not incident transverse to their surfaces and can be spread over their whole surface even the back side due to spinning and/or internal convection. In this case droplets and jets can have a large advantage over the slab case. This finding is contrary to some of the prior work and is due to self-shielding, circulation and geometric effects, which are neglected. Another unpublished study (Mahdavi and Schaffer, 1998) favored droplets.

Finally, there have been concepts using moving surfaces to get more heat transfer area. Spinning a cylinder exposes 3.14 times more area and eliminates the peak to average power hot spot problem (Yoshikawa, 1980). The idea of using spinning cylinders partly motivated the study of spinning liquid jets in this paper.

We will treat the divertor for a tokamak called ARIES-AT whose toroidal field is an order of magnitude larger than the poloidal field. We treat the plasma flux in the divertor region as free streaming particles strongly guided by the strong magnetic field in the "free molecular flow" way of thinking. This requires the collision mean free path to be long compared to the droplet or jet diameter. This condition is often violated, which in the future will require a more complicated analysis including viscous flow. It should be noted that gas collisions will transport power to the hidden surfaces of jets and droplets, further increasing their advantage over moving slabs.

In the case of the ARIES-AT tokamak, the plasma in the edge region and divertor region is described in Rognlien and Rensink (2001). Fig. 1 shows the configuration they analyze. Fig. 2 is a close-up of the divertor plate tilted at 30° to the poloidal field component and Fig. 3 is the power per unit area of the divertor plate. We will analyze the divertor plate replaced with an array of jets in one case and droplets in another case. Droplets are made from jets by imposing an acoustic pressure wave in the nozzle's reservoir to force the jets to pinch off into regularly spaced droplets.

We have considered the case of the divertor for a spheromak, a Field Reversed Configuration and a tandem mirror elsewhere (Moir et al., 2002), (Moir et al., 2001) and (Moir and Rognlien, 2007).

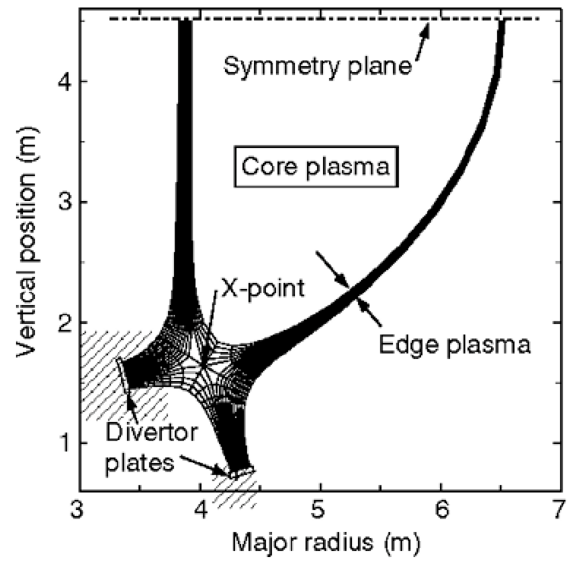

Fig. 1. The double-null configuration of the ARIES-AT is shown with the lower half only. This is Fig. 6 of Rognlien and Rensink (2002).

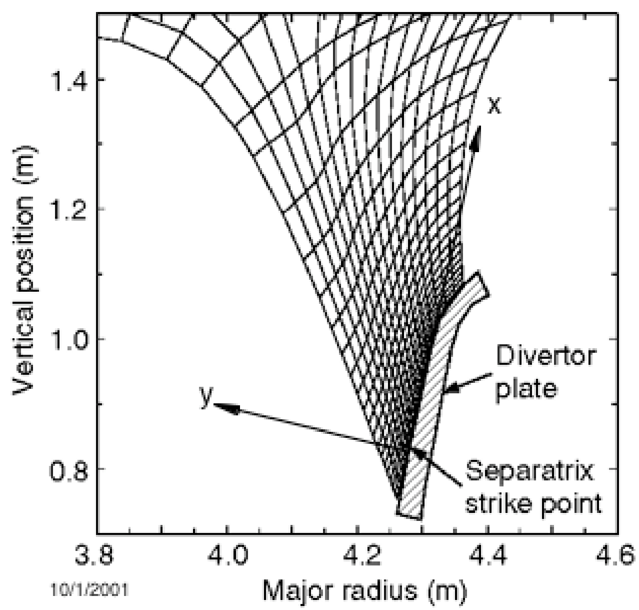

Fig. 2. The outer divertor plate tilted at ~30° between the poloidal flux and the plate (Fig. 10 from Rognlien and Rensink, 2002).

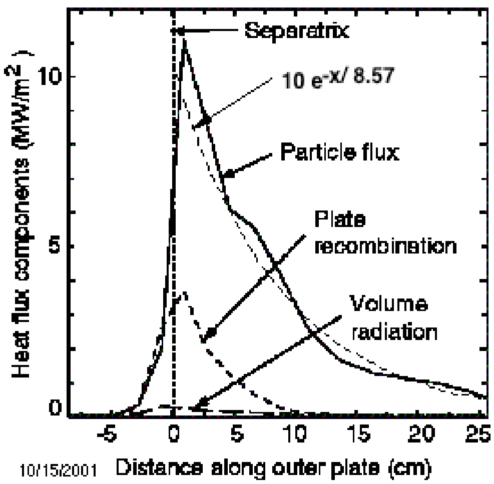

Fig. 3. The heat flux on the plate along the x-axis. (Fig. 12 from Rognlien and Rensink, 2002, for a high radiating edge plasma).

The heat flux on the plate from Fig. 3 for θ=30°, which will be used as the reference case for this study, is approximated as:

$$\Gamma = 0 \qquad x < 0$$

$$\Gamma = 10\frac{MW}{m^2}e^{-\frac{x}{0.0857m}} \qquad 0 < x < 0.25 \text{ m} \tag{1}$$

$$\Gamma = 0 \qquad x > 0.25 \text{ m}$$

If the divertor plate were tilted at an arbitrary angle, then the heat flux on the plate would be:

$$\Gamma = 0 \qquad x < 0$$

$$\Gamma = \sin\theta \cdot 20\frac{MW}{m^2}e^{-\frac{x}{0.04285m/\sin\theta}} \qquad 0 < x < 0.125 \text{ m}/\sin\theta \tag{2}$$

$$\Gamma = 0 \qquad x > 0.125 \text{ m}/\sin\theta$$

The average heat flux $\overline{\Gamma}$ is

$\overline{\Gamma} = \dfrac{\int \Gamma dx}{\int dx}$ = 6.485 sinθ in MW/m^2. Liquid divertors will likely be forced to be single null at the bottom. This would require us to double the powers above, but this has not been done in this study. The total power to the divertor is $P_{total} = \int 2\pi r \Gamma dx \approx 2\pi 4.3\,m \times 6.485 \times 0.125\,m = 21.9\,MW$.

An advantage of a liquid divertor is that failure to remove heat will cause excess evaporation and extinguish the fusion plasma rather than causing the divertor to melt. A disadvantage is the liquid is messy, corrosive and can cause contamination of the machine and is unfamiliar. If liquid walls are employed then a liquid divertor practically becomes a necessity as previously mentioned.

Geometric arrangement-Orientation of the divertor and jets

We will replace the solid divertor plate with rows of jets or droplets in the same plane as the solid plate of Fig. 2. These are shown in Fig. 4 and 5 with the coordinate system shown. For the ARIES-AT tokamak the field components at the divertor plate are 0.63 T poloidal field and 7.0 T toroidal field.

$$\phi = Tan^{-1}\frac{B_p}{B_T} = 5.14^0 \tag{3}$$

$$\psi = Tan^{-1}(\frac{B_P\,Sin\,\vartheta}{B_T}) = Tan^{-1}(Sin\,\phi\,Sin\,\vartheta) \tag{4}$$

θ is the angle between the poloidal field and the divertor plate plane.
ϕ is the angle between the total field and toroidal field.
ψ is the angle between the projection onto the Y-Z plane of the total field and the toroidal field.
ω is the angle between the z axis and the direction of the jets.
ω−π/2 is the angle between the toroidal field and the projection onto the x-z plant of the total field.
For our reference case shown in Fig. 4, the angles, θ=30°, ϕ=5.14°, ω=90° and ψ=2.58°. For the angles θ=90°, ω=0°, ψ=ϕ=5.14° and the liquid path length is

$\frac{0.125\,m}{\sin 5.14°} = 1.4\,m$, where the jets are directed along the plasma flow direction, however, the jets can not be injected owing to the interference with the plasma flow itself. For ω=90° and θ=90°, ϕ=ψ=5.14°. This case is the smallest exposure time (minimum path length of 0.125 m) as the liquid crosses the divertor.

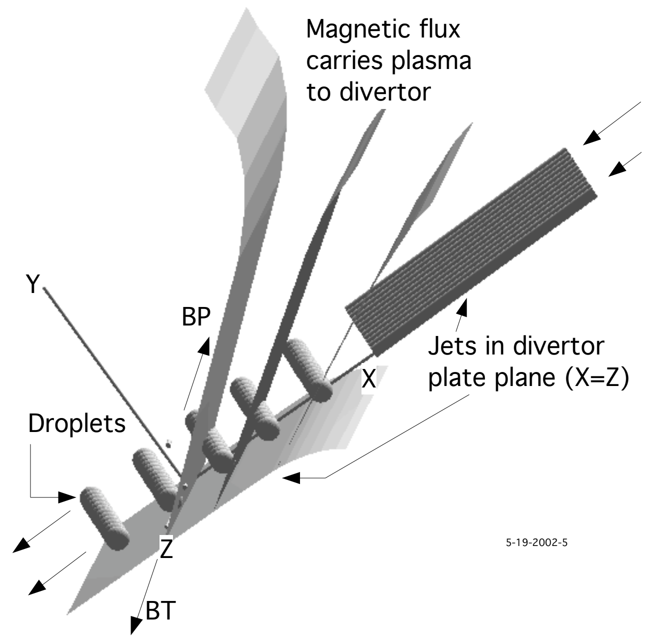

Fig. 4. Arrays of jets in the X-Z plane that can be made to break up into droplets replace the usual divertor plate (see Fig. 2). For small angle, θ<30°, one layer of droplets can intercept all the power. The figure is not to scale, as the droplets are smaller than a millimeter diameter.

The liquid might be moving at a speed of 10 m/s giving an exposure time of t.

For θ=30° and ω=90°

$$t = \frac{0.125\,m}{v\ Sin\,\theta\,Sin\,\omega} = \frac{0.125\,m}{10\,m/s \times \sin 30° \times Sin\,90°} = 0.0251\,s \qquad (5)$$

As one moves along with the fluid element, the distance, x varies with time:

$$x = \frac{0.125\,m}{\sin\theta \sin\omega} - v_0 t \sin\omega \tag{6}$$

The speed could be much higher perhaps 100 m/s limited by erosion of the nozzle surfaces, pumping power and high pressure in the reservoir feeding the nozzles.

The exposure time for θ = ω=90°, v= 10 m/s t= 0.0125 s
v= 100 m/s t= 0.00125 s

The magnetic field makes an angle ψ =5.14° from the plate. The peak flux normal to the plasma flow would be 20/tan 5.14°=222 MW/m^2 and the average would be 72.09 MW/m^2.

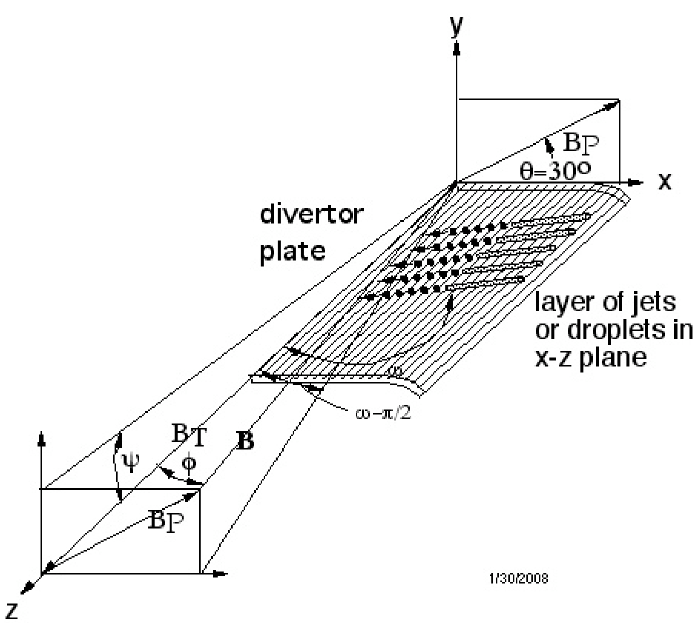

Fig. 5. The coordinate system for the jets, magnetic fields and divertor are shown.

The coordinate system shows the plasma flux follows the magnetic field and strikes the moving liquid with polar angles ϕ and θ. The divertor plate is replaced with jets or droplets in the x-z plane.

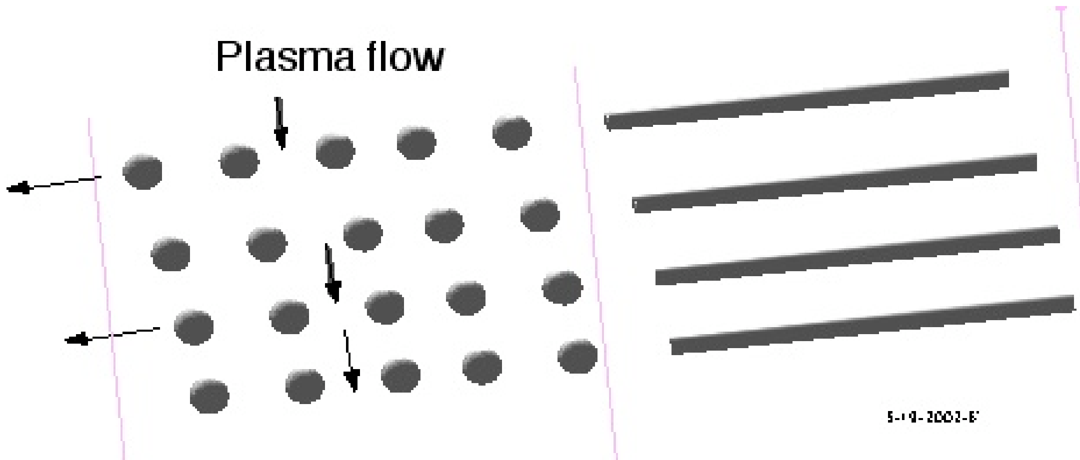

Fig. 6. Four layers of droplets are shown looking transverse to the droplet flow direction for θ=90°. The figure is not to scale, as the droplets are smaller than a millimeter diameter.

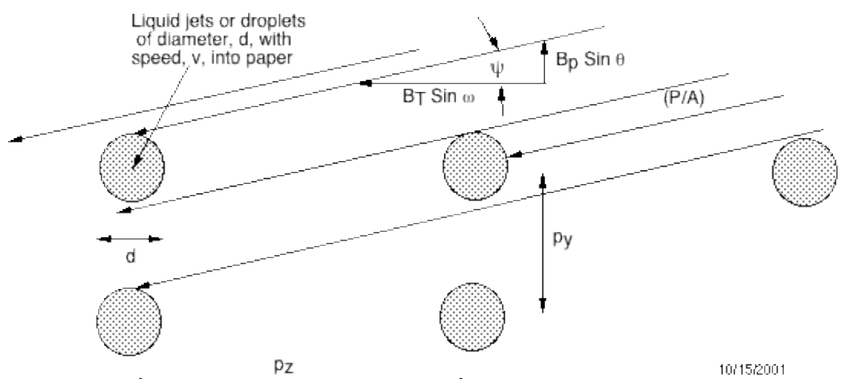

Fig. 7. The figure shows the y-z plane, which is looking in the direction of the liquid flow at the jets assuming no droplets formed.

Liquid jets can expose more surface area to the incident power flux by several means. The jets can be produced with rotation (spin) as they emerge from their nozzles. Thermal convection called "Marangoni or capillary" convection can cause circulation exposing (π+2) d more area than just the frontal area proportional to diameter, d. Finally, the jets can be made to break up into precisely sized and spaced droplets, exposing far greater surface to the power flux. Each of these effects will be discussed later.

Power distribution on the jets

In the case of jets, all the flux is intercepted on the first row when $\psi < \sin^{-1} d/p$. The power is averaged over the surface of the jet is then

$$\frac{P}{A}\sin\psi\frac{p}{\pi d} \qquad \text{for a spinning jet} \tag{7a}$$

$$\frac{P}{A}\sin\psi\frac{p}{(2+\pi)d} \quad \text{for Marangoni circulation.} \tag{7b}$$

When there is Marangoni circulation the increased area for heat transfer is about a factor of five. When the jet is simply spinning then the increase is only a factor of π.

For $\psi = 2.58°$ and $(P/A)_{peak} = 222$ MW/m^2, the peak power average over a jet is 3.18 p/d MW/m^2 for spinning jets and 1.95 p/d MW/m^2 for Marangoni circulation. The ratio d/p can range from $\sin\psi = 0.045$ to 1 giving an average power per unit area of 3.18 to 70.7 MW/m^2 for spinning jets and 1.95 to 43.4 MW/m^2 for Marangoni convection. The lower value corresponds to jets just touching.

In the case when $\psi > \sin^{-1} d/p$, the first row of jets do not intercept all the power and multiple rows as shown in Fig. 6 are needed. Also when droplets are formed as shown in Fig. 4 multiple rows of jets are called for. Multiple rows raise the power handling ability and will be discussed later.

For a slab for 30° our reference case has a peak power $(P/A)_o$ of 10 MW/m^2. For close packed jets the lowest value of p/d is probably 2 giving 3.9 to 6.36 MW/m^2 for the spinning or Marangoni convection jets. This would be a factor of 1.6 to 6.36 times the heat transfer area of a moving slab.

When the incident flux is aligned in the direction of the liquid flow (θ=90, ω=0) then only the normal component of power flux comes in, 20 MW/m^2 peak power flux and 6.485 MW/m^2 average in our reference case with θ=90°.

Internal Circulation or convection in jets and droplets

Jets or droplets are warmed up on their exposed side as shown in Fig. 11**.** The differential surface tension between warm and cool sides sets up internal circulation so that heat is effectively spread over a larger area and penetrates a thermal diffusion distance into the liquid, x_{th} in a thermal diffusion time. The power is in effect spread over the surface area of the droplet or jet. In addition, the internal circulation exposes the interior of the droplet as well. A round jet then has an outer area of πd plus an internal area of 2d (heat diffuses two ways) compared to the frontal area proportional to d. This area depends on the circulation being fast enough. The transit time across the divertor plasma is 25 ms in our reference case (10 m/s and θ=30°).

Internal circulation in a jet, cylindrical case

The stream lines shown in Fig. 8 obey the cylindrical vortex formula from Lamb (1932)[1]:

$$\Psi = J_1(kr)\sin(\theta) \tag{8}$$

$$k=3.8317 = \text{first root of } J_1 \tag{9}$$

Ψ varies from 0 to 0.5819. The circle is Ψ=0 and the largest value of Ψ is 0.5819 at normalized radius=0.4805.

The incident power is spread over a larger area:

$$\frac{P}{A} = \left(\frac{P}{A}\right)_0 \left(\frac{1}{\pi + 2}\right) = \frac{1}{5.14}\left(\frac{P}{A}\right)_0 \qquad \text{round jets} \tag{10}$$

If there is incident power spreading by some effect such as spinning or plasma diffusion by collisions but no internal circulation, then the factor 5.14 becomes 3.14.

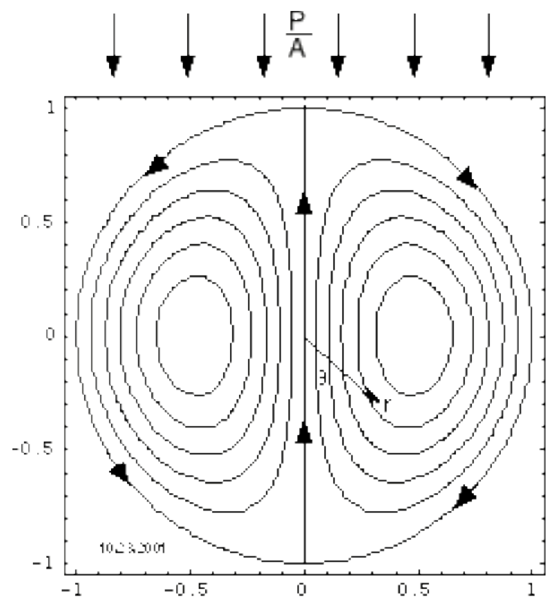

Fig. 8. Internal circulation is shown for a vortex in cylindrical geometry appropriate for a jet (courtesy of Ed Morse). Flux values plotted are 0.0, 0.1, 0.2, 0.3, 0.4, and 0.5.

1. The velocity field is such that when immersed in an infinite liquid the vortex propagates at speed v and the surface speed at the edge is a maximum of -2v.

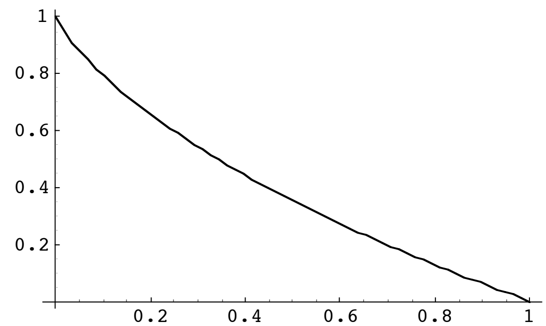

Fig. 9. The normalized volume enclosed within the flux surface is plotted versus the normalized flux for the cylindrical vortex (courtesy of Ed Morse).

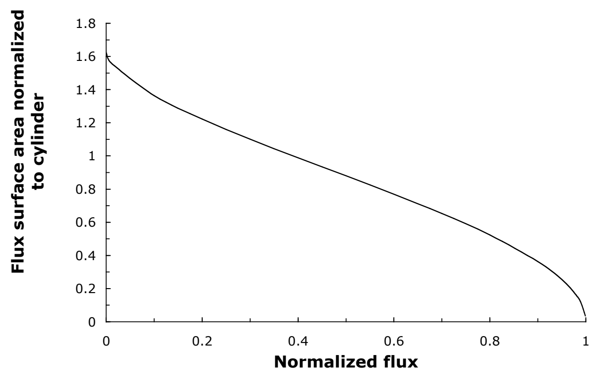

Fig. 10. The surface area of both left and right companion flux surfaces normalized to the surface of a cylinder is plotted versus the normalized flux for the cylindrical vortex (courtesy of Ed Morse).

The calculation of surface area is 1.637. When normalized to the frontal area of a cylinder this becomes 5.14, agreeing with Eq. 10.

Internal circulation in a droplet, spherical case

Circulation inside a droplet form streamlines shown in Fig. 14 that obey the Hill's vortex formula[2].

2. The velocity field is such that when immersed in an infinite liquid the vortex propagates at speed v and the surface speed at the equator is –1.5v.

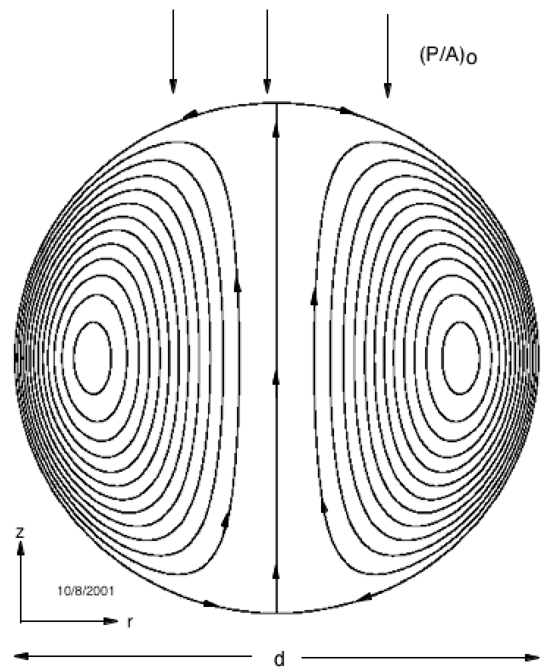

Fig. 11. Droplets with internal circulation shown for the Hill's vortex in spherical geometry appropriate for a droplet (courtesy of Dick Bulmer and Ed Morse).

$$\Psi = r^2(1 - r^2 - z^2) \tag{11}$$

Ψ varies from 0 to 0.25. The circle is Ψ=0 and the largest value of Ψ is 0.25 at normalized radius=$1/(2)^{0.5}$.

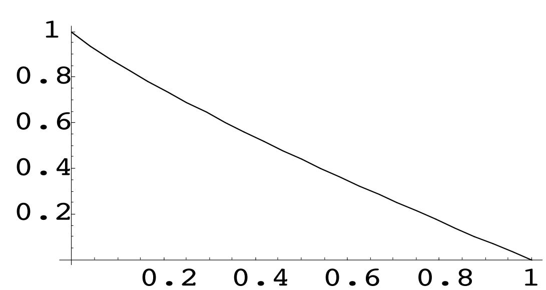

Fig. 12. The normalized volume enclosed within the flux surface is plotted versus the normalized flux (courtesy of Ed Morse).

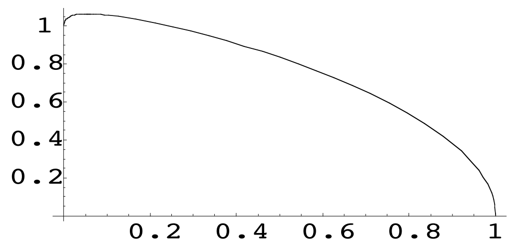

Fig. 13. The normalized surface area of each flux surface is plotted versus the normalized flux (courtesy of Ed Morse).

In the case of droplets, the frontal area is $\pi d^2/4$, whereas the surface area is πd^2 plus some area in the interior due to circulation, which from Fig. 13 is estimated at about 7% additional area. The incident power is spread over a larger area:

$$\frac{P}{A} \approx \frac{1}{4 \times 1.07}\left(\frac{P}{A}\right)_0 \approx \frac{1}{4.3}\left(\frac{P}{A}\right)_0 \qquad \text{droplets} \qquad (12)$$

If there is incident power spreading by some effect such as spinning or plasma diffusion by collisions but no internal circulation, then the factor 4.3 becomes 4.

Temperature dependent circulation-the Marangoni effect

One of the driving forces for the circulation is temperature dependent surface tension, σ(T), which is called the Marangoni effect or thermal capillarity. The liquid is pulled from the hot surface exposed to the power flux to the cold region, which is shadowed from the power flux and where the surface tension is larger. The circulation speed v is limited by viscous flow dissipation and the front to back temperature difference.

We will estimate the steady flow speed and then the time for the flow to establish or decay after the heating stops.

Oliver and DeWitt (1988) treat a case that is closely related to our interest. A laser is assumed to deposit heat onto a droplet. Flow inside the droplet is driven by the Marangoni effect. The surface tension in the heated region is weaker than in the shadows and this imbalanced force sets up convection just balanced by viscous forces. The exterior gas is assumed to remove heat at the rate it arrives so a steady state is established. The flow speed at infinity is 2/3 that at the equator. Assuming the external gas flow is of low viscosity and thermal conductivity the Olive and DeWitt result is:

$$\mathrm{v}_\infty = -\frac{\partial \sigma}{\partial T}\frac{P/A \times a}{9k\eta} = 1.2\times 10^{-4}\,\frac{N}{mK}\,\frac{10^6\,W\,0.4\times 10^{-3}\,m}{9\times 1.06\dfrac{W}{mK}0.008\,Pa\cdot s} = 0.6\,m/s \tag{13}$$

The surface flow speed at the equator of the droplet is 0.9 m/s for an 8 mm dia droplet of flibe with a nominal heat load of 1 MW/m^2 coming from one side on an unshadowed droplet.

When the power flux is reduced owing to shadowing by other droplets the circulation speed will be reduced. Sadhal, Trinh and Wagner (1992) come up with the same formula above with the term multiplying it to account for this reduced area of heating:

$1\text{-}\cos^3\theta_0$

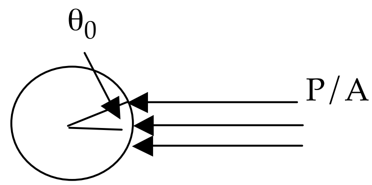

For θ_0=20° this factor becomes 0.17 for example.

The time for surface tension driven circulation on the surface to spread to the interior has been estimated by Schrock (1998) where he compares the process to decay of laminar flow in a tube. His result for 90% decay of the flow is

$$t = 0.5\frac{a^2}{\nu} = 0.5\frac{a^2\rho}{\eta} = 0.5\frac{(0.0005\,m)^2 1900\,kg/m^3}{0.008\,Pa\cdot s} = 0.03\,s$$

This time is longer than the transit time across the divertor for most of our examples so we might want to use droplets of diameter smaller than 1 mm if we need to utilize fully developed laminar flow inside the droplets. The e-folding time would be 13 ms.

The surface speed and time to achieve a steady flow is shown in Fig. 14 for droplets of 0.5 mm diameter and a heat flux from one side of a nominal 1 MW/m^2.

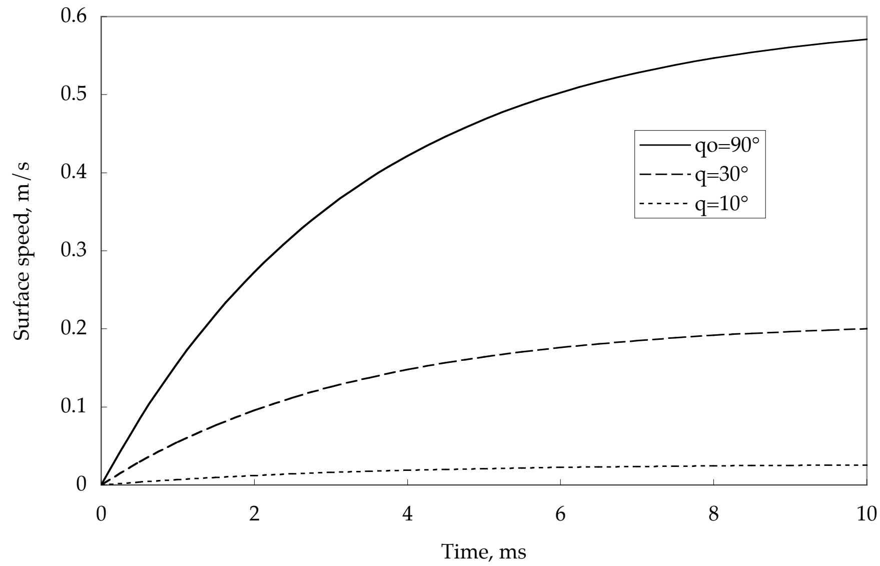

Fig. 14. Time dependent convective surface speed.

The surface tension for flibe is (Yajima, Moriyama, Oishi and Tominaga, 1982):

$$\sigma_{flibe}(500\ {}^0C) = 0.20 - 1.2 \times 10^{-4}(T - 500\ {}^0C) \tag{14}$$

As an example, if the temperature front to back were 50 °C, the circulation surface speed would be:

$$\mathrm{v} = \frac{1.2 \times 10^{-4} \times 50}{2\pi 0.008 Pa \cdot s} = 0.12\, m/s$$

To enhance heat transfer by Marangoni convection the surface must circulate a number of times during the exposure time; let's say five times. This sets another criterion on droplet size or circulation surface speed.

$$d < \frac{vt}{5(1+\pi/2)} \quad \text{or equivalently} \quad v > \frac{d}{t}5(1+\pi/2) \tag{15}$$

where t is the exposure time, which is the time for the droplets to transit the divertor zone and v is the surface tension driven surface speed from Eq. 27. Typical droplet speed might be 10 m/s giving a 0.025 s exposure time for a 0.25-m path across the divertor. For a 1 mm dia jet we want v>0.5 m/s. The temperature difference from front to back can be estimated from Eq. 20 using t=0.005 s.

This speed may be overly restrictive but should ensure good surface heat dispersal.

This surface circulation will be driven by a number of effects: Marangoni convection, velocity shear in the formation process, MHD effects which both retard and enhance circulation (Tillack, 2001).

Dimensionless numbers

The Reynolds number, $\mathrm{Re} = \frac{\mathrm{v}\, d\, \rho}{\eta}$ For a mm dia droplets of flibe at 0.4 m/s,

$\mathrm{Re} = \frac{\mathrm{v}\, d\, \rho}{\eta} = \frac{0.4\ \mathrm{m/s} \times 0.001\ \mathrm{m} \times 2000\,\mathrm{kg/m^3}}{0.008\, Pa\, s} = 100$ The transition to turbulence usually occurs for Reynolds number between 1000 and 2000 so we might expect the convection to be laminar.

The Prandl number, Pr, is the ratio of momentum diffusivity to thermal diffusivity.

$$\mathrm{Pr} = \frac{\mathrm{C}\eta}{k} = \frac{0.008\, Pa \cdot s \times 2380\,\mathrm{J/kgK}}{1.06\, W/mK} = 18$$

The Capillary number, Ca, is the ratio of viscous force to surface tension force.

$Ca = \frac{\eta v}{\sigma} = \frac{0.008\, Pa \cdot s \times 1 m/s}{0.17 N/m} = 0.047$. We expect the surface tension to quickly develop a surface flow.

The Weber number, We, is the ratio of inertial force to surface tension force.

$We = \frac{\mathrm{d}_d v^2 \rho}{\sigma} = \frac{0.001 m \times (1 m/s)^2 \times 1900 \mathrm{kg/m^3}}{0.17 N/m} = 11$. We can expect a 1 mm dia drop with a surface speed of 1 m/s will probably fly apart. The speed and size will need to be lower.

Surface tension limited spin of jets and droplets

Another way the power can be dispersed over the surface is by spinning the jets as it comes out of its nozzle. How fast can the surface speed be without the jet flying apart due to insufficient surface tension? Any mechanism that causes internal circulation such as Marangoni convection or MHD driven convection will have speed limitations due to surface tension breaking in addition to other limitations.

$$\mathrm{v}_s = \left(\frac{3\sigma}{\rho r}\right)^{1/2} \tag{16}$$

=surface speed of a spinning cylindrical jet where the outward force is just balanced by surface tension and represents an upper limit to spin rate. Instabilities will set a spin limit even lower.

$$\mathrm{v}_s < \left(\frac{3 \times 0.2}{2000 \times 0.4 \times 10^{-3}}\right)^{1/2} = 0.87 m/s \text{ for flibe jet of 0.4 mm radius.} \tag{17}$$

$$v_s < \left(\frac{3 \times 0.4}{6000 \times 3.6 \times 10^{-3}}\right)^{1/2} = 0.24\, m/s \text{ for SnLi jet of 3.6 mm radius.} \qquad (18)$$

Using a surface tension of 0.2 N/m for flibe and 0.4 N/m for SnLi. The circulation speed for flibe may be adequate but it appears to be much too slow for SnLi based on the discussion in the next section.

If we set the surface energy equal to the kinetic energy of rotation we get:

$$v_s = \left(\frac{8\sigma}{\rho r}\right)^{1/2} \qquad (19)$$

It is curious that this speed is 1.6 times larger than that above.

For the sphere the kinetic energy of rotation is $\frac{4\pi\rho v_s^2\, r^3}{15}$ and the surface energy is $4\pi r^2 \sigma$. Equating these gives a surface speed $v_s < \left(\frac{15\sigma}{\rho r}\right)^{1/2}$

$$v_s < \left(\frac{15 \cdot 0.2}{2000 \cdot 0.4 \times 10^{-3}}\right)^{1/2} = 1.9\, m/s \text{ for flibe jet of 0.4 mm radius.}$$

$$v_s < \left(\frac{15 \cdot 0.4}{6000 \cdot 3.6 \times 10^{-3}}\right)^{1/2} = 0.53\, m/s \text{ for SnLi jet of 3.6 mm radius.}$$

Apparently flibe jets or droplets can circulate fast enough to spread the heat load over the full area but SnLi jets or droplets might fly apart at the necessary speeds. However, liquid metal jets or droplets have so much less evaporative flux that smaller diameters can be used. Then as will be shown, the heat will reach the center and the more complete heat transfer solution will be needed.

Time dependent surface temperature

The temperature on the surface of a droplet or jet will be fairly constant if surface tension driven convection is sufficiently strong (as will be shown later). Then, the surface temperature will increase with time depending on the heat transfer into the liquid interior according to the infinitely thick slab formula:

$$T(t) = T(t=0) + 2\frac{P}{A}\left(\frac{t}{\pi\rho kc}\right)^{0.5} \qquad \text{infinite slab} \qquad (20)$$

for a slab of thickness a this formula is:

$$T(t) = T(t=0) + \frac{P\,a}{A\,k}\left(\frac{\alpha t}{a^2} + \frac{1}{3} - 2\sum_{n=1}^{\infty}\frac{e^{-\frac{(n\pi)^2\,\alpha\,t}{a^2}}}{(n\pi)^2}\right) \qquad \text{slab finite thickness} \quad (21)$$

and for a cylinder of radius a is:

$$T(t) = T(t=0) + \frac{P\,a}{A\,k}\left(\frac{2\alpha t}{a^2} + \frac{1}{4} - 2\sum_{n=1}^{\infty}\frac{e^{-\frac{\lambda_n^2\,\alpha\,t}{a^2}}}{\lambda_n^2}\right) \qquad \text{cylinder} \qquad (22)$$

Where λ_n are the roots of the Bessel function, $J_1(\lambda_n) = 0$

and for the spherical formula:

$$T(t) = T(t=0) + \frac{P}{A}\left(\frac{3t}{\rho ca} + \frac{a}{5k} - \frac{2a}{k}\sum_{n=1}^{\infty}\frac{e^{-\frac{\beta_n^2\,\alpha\,t}{a^2}}}{\beta_n^2}\right) \qquad \text{sphere} \qquad (23)$$

from Carslaw and Jaeger (1958).

For t very close to zero the terms in the sum converge very slowly; however, for t slightly larger than zero only the first term is important and even that term is quite small. The formula for the temperature on the surface of a sphere differs from the slab formula for surprisingly small times. We expect to use the slab formula only for times small compared to the thermal diffusion time with corrections as can be seen in Fig. 15.

$$a = d/2 \tag{24}$$

$$\alpha = \frac{k}{\rho c} = \textit{thermal diffusivity} \tag{25}$$

$$\beta_n = \tan\beta_n \tag{26}$$

$$\beta_1 = 4.494, \beta_2 = 7.725, \beta_3 = 10.904, \beta_4 = 14.066, \ldots\ldots \beta_n \approx (n+1/2)\pi \tag{27}$$

$$t' = \frac{\alpha t}{a^2} \tag{28}$$

$$\frac{T(t) - T(t=0)}{\frac{a}{k}\frac{P}{A}} = 2\left(\frac{t'}{\pi}\right)^{1/2} \qquad \text{infinite slab} \tag{29}$$

(19)

$$\frac{T(t) - T(t=0)}{\frac{aP}{kA}} = \left(t' + \frac{1}{3} - 2\sum_{n=1}^{\infty}\frac{e^{-(n\pi)^2 t'}}{(n\pi)^2}\right) \qquad \text{finite slab} \tag{30}$$

$$\frac{T(t) - T(t=0)}{\frac{aP}{kA}} = \left(2t' + \frac{1}{4} - 2\sum_{n=1}^{\infty}\frac{e^{-\lambda_n^2 t'}}{\lambda_n^2}\right) \qquad \text{cylinder} \tag{31}$$

$$\frac{T(t) - T(t=0)}{\frac{a}{k}\frac{P}{A}} = \left(3t' + 1/5 - 2\sum_{n=1}^{\infty}\frac{e^{-\beta_n^2 t'}}{\beta_n^2}\right) \qquad \text{sphere} \tag{32}$$

In the Tillack and Zhou (1998) paper there is a simpler formula for the spherical case which is accurate for t′ up to 0.5 after which it diverges rather than approach a straight line as it should.

$$\frac{T(t)-T(t=0)}{\frac{a}{k}\frac{P}{A}} = e^{t'}\left(1+erf\sqrt{t'}\right)-1 \qquad \text{Tillack and Zhou sphere formula} \qquad (33)$$

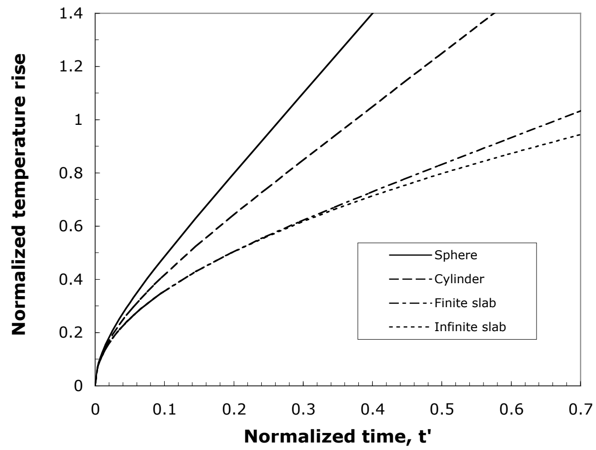

Fig. 15. Surface temperature rise for a sphere, a cylinder, a finite thickness slab and an infinite slab.

$$t' = x_{th}^2 / a^2 \qquad (34)$$

Table 1

t'	x_{th}/a
0	0
0.01	0.1
0.04	0.2
0.09	0.3
0.16	0.4

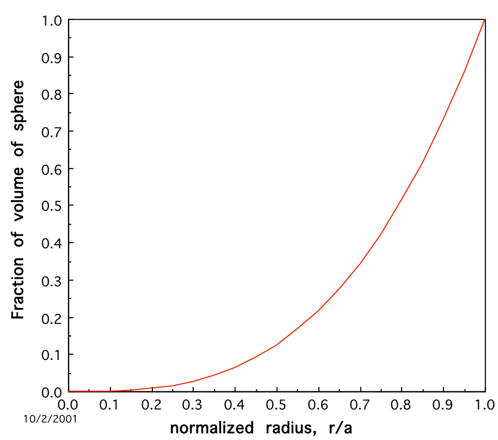

Fig. 16. Volume fraction of a sphere versus the normalized radius.

We can see from Fig. 16 that half of the spherical volume is heated when t' is less than 0.05 and the error there in using the slab formula is only 19%. We can multiply the slab formula by 1+1.35t' to make a correction for the spherical application without the complications of the spherical formula, which is valid as long as the liquid surface locally looks flat and where T is temperature, t is time, k is thermal conductivity is density, and c is heat capacity. The droplet size must be greater than the thermal diffusion distance by about a factor of 5 for us to use the slab formula without corrections of less than 20%. This requires

$$d \geq 5\, x_{th} \tag{35}$$

$$x_{th} = (\alpha\, t)^{1/2} \tag{36}$$

Time of interest for cooling the divertor might be (0.25 m/10 m/s) 0.025 s depending on orientation angles shown in Fig. 4. The thermal diffusion distance and droplet sizes for using the slab formula are given in Table 2.

Table 2

Parameters of candidate liquids

Liquid	C, J/kgK	ρ, kg/m^3	k, W/mK	η, Pa•s	σ, N/m	x_{th}, mm	a=5x_{th} mm
Flibe	2380	1900	1.06	0.008	0.17	0.08	0.4
Li	4360	450	53*	0.0004	0.28*	0.82	4.1
SnLi	318	6000	40 *		0.5	0.72	3.6
PbLi	160	8700	15*	0.0011	0.43*	0.52	2.6
Ga	380*	5900	60*		0.7	0.82	4.1
Sn	230*	5700	35 *	0.0011	0.53*	0.82	4.1

*500 C°

For the short times of interest the simple slab formula is sufficiently accurate for our purposes and a simple correction as previously note could make it even more accurate with a small correction.

We can see the temperature rise with time will be decreased by a factor of 5.14 over that of a slab for the case with close packet jets. The area the incident power is spread over for other configurations will be discussed later.

Evaporation rates

Evaporation from a surface into a vacuum is given by

$$J = \frac{n\overline{\mathrm{v}}}{4}, \quad \overline{\mathrm{v}} = \sqrt{\frac{8kT}{\pi m}}, \quad n = \frac{P}{kT}, \quad J = \frac{P}{kT}\frac{\sqrt{\frac{8kT}{\pi m}}}{4} = \frac{P}{(2\pi mkT)^{0.5}} \tag{37}$$

$$P = e^{(A-B/T)} \tag{38}$$

$$J = CT^{-0.5}e^{(A-B/T)} \tag{39}$$

$$C = 1/\sqrt{2\pi\, m\, k}$$

$$C = 1/\sqrt{2\pi\, 6.941 \times 1.674 \times 10^{-27} \times 1.3804 \times 10^{-23}} = 0.3828 \times 10^{24} \text{ for Li}$$

for flibe BeF_2; m=9.01218+2×18.9984=47.00898

The flibe vapor pressure used is $\log_{10} P_{torr} = 9.424 - 11026.208/T(K)$ (Olander, Fukuda and Baes, Jr, 2003 and Zahgloul, Sze and Raffray 2003) and is converted to Pascals by multiplying by 133.3. This latest estimate of evaporation rate is about a factor of three lower than previous estimates in the 500 °C region. It is about the same in the region of 1000 °C, where the original data were taken.

$$P(Pa) = \exp(26.592 - 25389/T)......Li_2BeF_4....BeF_2 \ evaporation \tag{40}$$

$$P(Pa) = \exp(22.16 - 17220/T)......Li............Li \ evaporation \tag{41}$$

$$P(Pa) = \exp(24.81 - 25800/T).....Sn_{80}Li_{20}....Li\ evaporation \qquad (42)$$

Table 3

Evaporation parameters

Liquid	A	B	C, 10^{24}
Flibe	25.592	25389	0.3828
Li	22.16	17220	0.9961
SnLi	24.81	25800	0.9961

Slab as a reference

We will assume a constant heat flux, which is what our heat transfer equations assume. For θ=30° the average heat flux on the surface of a slab is 3.24 MW/m^2. For reference we treat the slab case with speed, 10 m/s and ω =90° in Fig. 4. Using the slab formula for surface temperature rise and using the evaporation formulae we get the space dependent evaporation results for the slab case plotted in Fig. 14. The average flux is:

$$J_{ave} = \frac{\int J dx}{\int dx} \qquad (43)$$

$$\int dx = 0.125\ m \sin\theta \qquad (44)$$

We define the average flux referred to 90° cross section as

$$J_{90} = J_{ave}/\sin\theta = \frac{\int J dx}{0.125\ m}$$

(45)

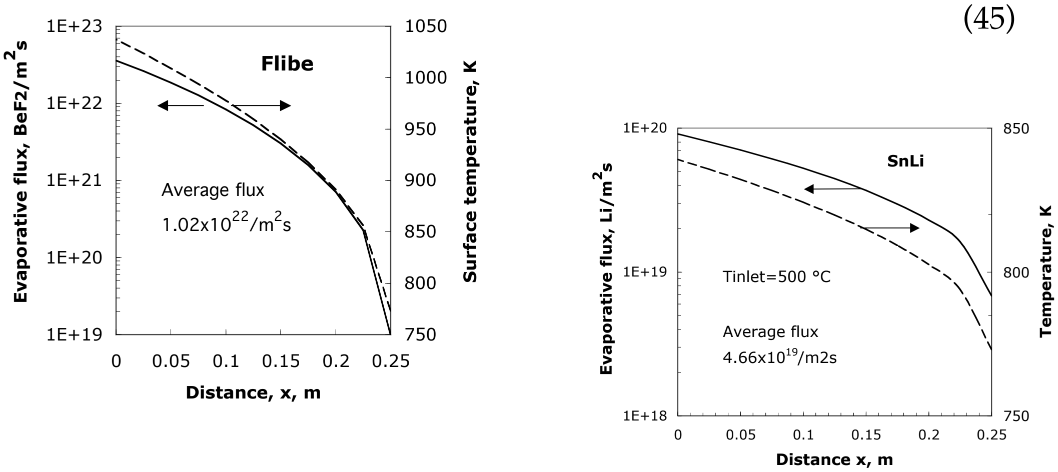

Fig. 17. Evaporative flux for slab geometry with v= 10 m/s and θ=30°. The liquid travels from right to left.

The average flux is a function of angle θ and minimizes at a small angle for flibe and at about 30° for SnLi as can be seen in Fig. 18.

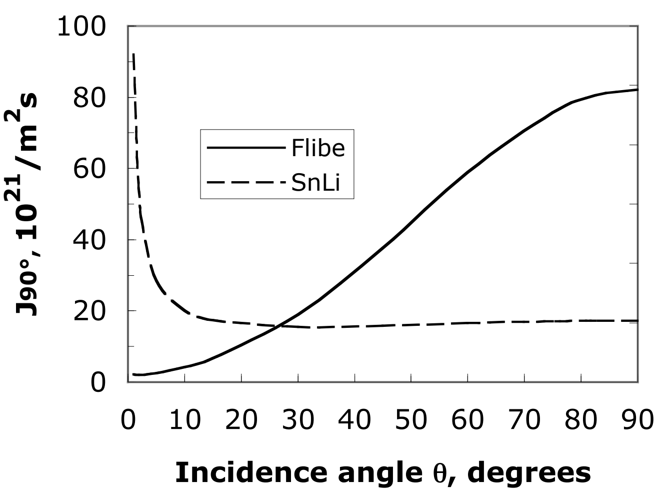

Fig. 18. Flux referred to 90°.

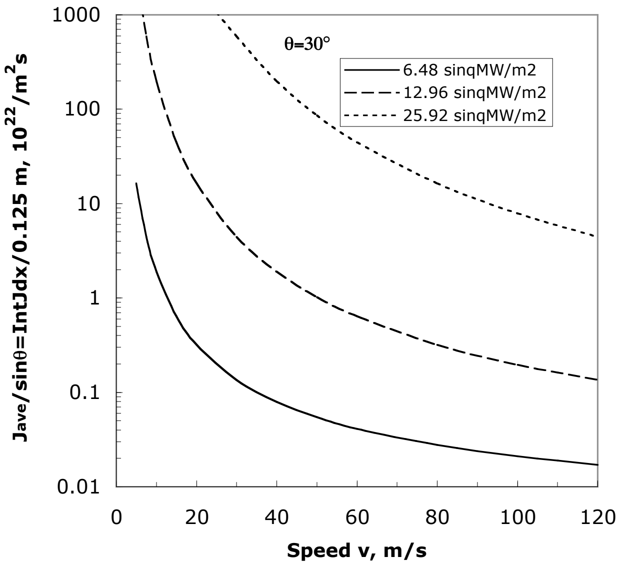

Fig. 19. The evaporative flux versus liquid speed and power density is given.

From one case we can scale to other cases as follows:

$$J_{ave} \propto f(\frac{P/A}{v^{0.5}}) \tag{46}$$

that is, given the average flux at one P/A and speed of liquid we can get the same value to double the power flux at four times the speed.

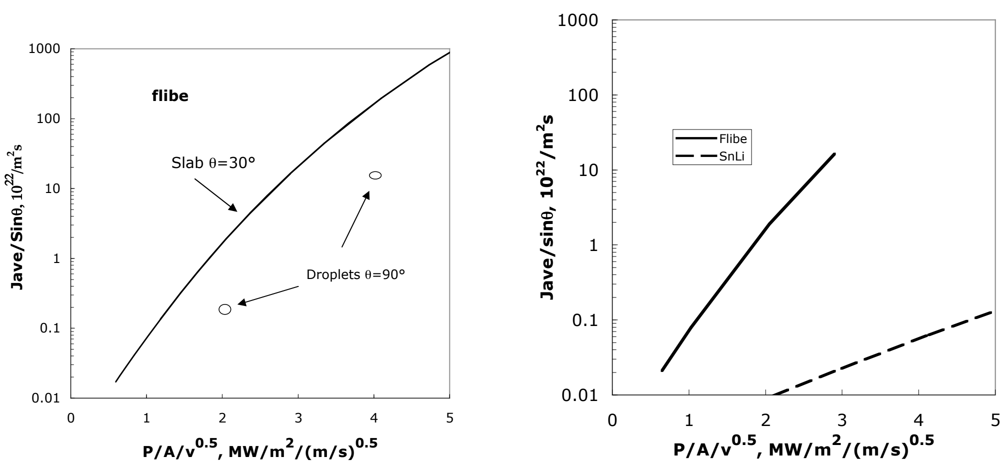

Fig. 20. Evaporative flux. Note that SnLi can handle a factor four or so more power than flibe for the same evaporation.

For flibe we come up with an analytic fit to the plot above where x= $\frac{P/A}{v^{0.5}}$

$$J/\sin\theta = e^{0.014x^3 - 0.3575x^2 + 4.0745x - 6.3496}. \tag{47}$$

The value "/A that is used is the 90° value (6.385 MW/m^2 for the reference case).

Temperature rise and pumping power for jets and slabs

The average temperature rise of a slab of thickness δ is

$$\Delta T = \frac{6.48\,MW/m^2 \times 0.125\,m}{\rho v c \delta} = \frac{0.17\,K}{v\delta} \tag{48}$$

for v=10 m/s and d=1 mm $\Delta T = 17\,K$ whereas the surface temperature rise from the figure above for 30° is 264 K.

The ratio of pumping power to heat removed is

$$\frac{0.5\dot{m}v^2}{6.48MW/m^2 \times 0.125m} = \frac{0.5\rho\delta v^3}{6.48MW/m^2 \times 0.125m} = 1.23\times 10^{-3}\delta v^3 \tag{49}$$

For δ=1 mm and v=10 m/s the ratio is $1.23\text{x}10^{-3}$.

The average temperature rise of a layer of jets of spacing p is

$$\Delta T = \frac{6.48\,MW/m^2 \times 0.125\,m \times p}{\rho \frac{\pi}{4} d_j^2 v c} = \frac{0.217 \times p}{d_j^2 v} \tag{50}$$

where, owing to the shallow angle of incidence all the power is assumed to fall on the first layer of jets. For jet spacing $p=4d_j$, d_j =0.4 mm and 10 m/s

$$\Delta T = 217\,K$$

The ratio of pumping power to heat removed is

$$\frac{0.5\dot{m}v^2}{6.48MW/m^2} = \frac{0.5\rho\frac{\pi}{4}d_j^2 v^3}{6.48MW/m^2 \times 0.125m \times p} = \frac{0.97\times 10^{-3} d_j^2 v^3}{p}$$

For jet spacing $p=4d_j$, d_j =0.4 mm and 10 m/s the ratio is $1\text{x}10^{-4}$.

One-layer analysis for cylindrical jets

A row of jets as shown in Fig. 4 and 5 that have not broke up into droplets will intercept all the power as long as $\frac{d_j}{p} \geq \sin\psi = \sin 2.58^o = 0.045$ for our tokamak example, where $\psi = \tan^{-1}(\sin\vartheta \sin\varphi) = \tan^{-1}(\sin 30^o \sin 5.14^o) = 0.045$.

The power averaged over the surface of the spinning jet is the value over a slab times $\frac{p}{\pi d_j}$. If we assumed the Marangoni effect were convecting the surface into the interior then this factor would be $\frac{p}{(2+\pi)d_j}$. At a divertor plate of 30°, as shown in Fig. 2, we have an average power of 3.24 MW/m^2. This becomes 1.03 x p/d_j MW/m^2 on the surface of a spinning jet and $0.63\frac{p}{d_j} MW/m^2$ for Marangoni convection. For fairly close spaced jets the power density on its surface for a convecting jet is lower than for a slab.

We assume the evaporation on the side of the jet facing away from the plasma will condense on other surfaces and therefore will not contribute to contamination of the plasma. The net evaporative flux to be compared to that of a slab is the evaporative flux on the surface of the jet multiplied by the factor, $\frac{\pi d_j}{2p}$. We plot the evaporative flux for a single row of jets with variable spacing in Fig. 21. Note the evaporative flux for jets is less than that of a slab up to p/d_j=3.5 for flibe jets spinning, 6 for flibe jets convecting and 5 for SnLi for our example.

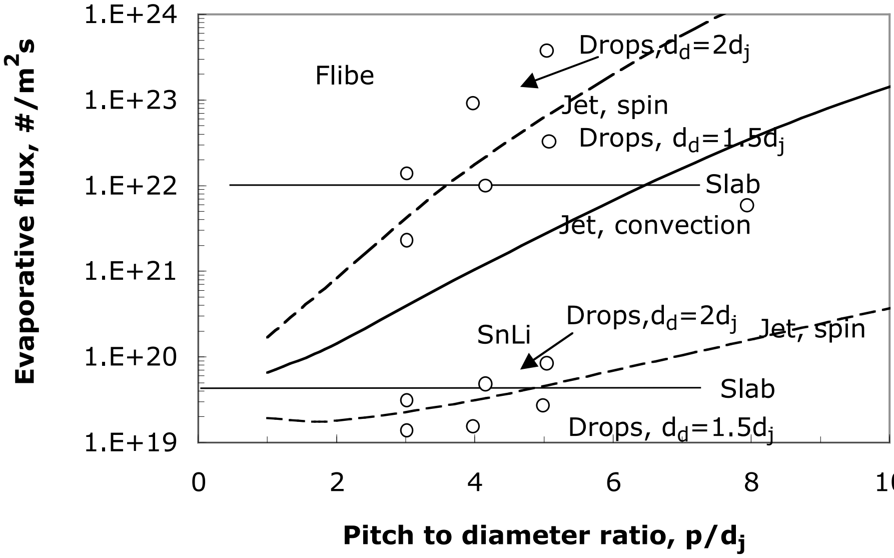

Fig. 21. The evaporative flux at θ=30° averaged over the divertor versus the jet's pitch to diameter ratio shows a reduced evaporation for jets compared to a slab (see Fig. 17), because the heat flux is spread over the entire jet surface due to spinning and only forward evaporation escapes.

In general, when $\frac{d_j}{p} \le \frac{\frac{B_p}{B_T}\frac{\sin\theta}{\sin\omega}}{1+\left(\frac{B_p}{B_T}\frac{\sin\theta}{\sin\omega}\right)^2}$, (51)

a multi-row analysis is called for.

Multiple row analysis is needed when $\frac{d_j}{p} \le 0.045$ *or* $\frac{p}{d_j} \ge 22.2$, however, we see from Fig. 21 that when p/d$_j$>22 the evaporation is very large and multiple layer analysis is not going to give a lower result for evaporation than for a slab. Therefore we do not treat the multilayer case for jets.

One-layer analysis for droplets

An array of jets can be made to form droplets that are precise in size and spatially aligned (coherent) from jet to jet. When $\theta \le \sin^{-1}\frac{d_d}{L}$ one layer of droplets intercepts all power because the droplets "look" like a continuous jet at low angles.

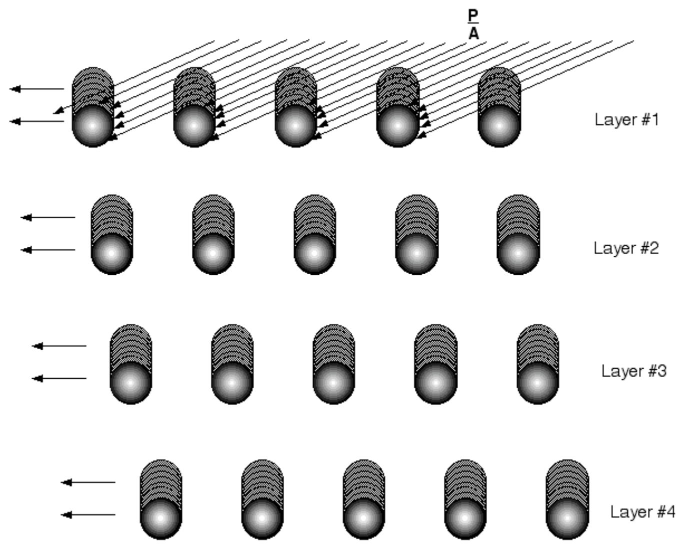

Fig. 22. One layer of droplets intercepts all the power for $\theta \le \sin^{-1}\frac{d_d}{L}$.

The average power P/A is 6.485×sinθ MW/m^2 assumed to be uniform for our calculation. P/A also equals $72\frac{MW}{m^2}\sin\psi$. The power intercepted by each droplet is

$$P_{drop} = \frac{P}{A} \times p \times L \tag{52}$$

$$\frac{P_{drop}}{area\ of\ drop} = \frac{P}{A} \times \frac{pL}{4\pi\frac{d_d^2}{4}} \tag{53}$$

The nozzle spacing p in a manifold could possibly be spaced as close as $p=2d_j$; but then with $d_d=2d_j$ the droplets would be touching. Every other jet could protrude by a distance of L/2 (half the spacing between droplets in the direction of flow) to avoid touching. A more practical minimum spacing might be $p=2d_d=4d_j$. We have only a little control over the minimum spacing between rows owing to manufacturing limits of how close each nozzle can be spaced.

The volume of a cylinder of length L equals the volume of a drop $L \times \pi d_j^2/4 = \frac{4}{3}\pi d_d^3/8$ where L is the spacing between droplets from a nozzle determined by the acoustic pressure inducer and jet speed as discussed in the section, "Acoustic frequency to make droplets."

$$L = \frac{2d_d^3}{3d_j^2} \tag{54}$$

For $L=4.5008d_j$ or equivalently $d_d=1.89d_j$ the most unstable perturbations of the jet as found by Rayleigh (Volker Kachel (1990). Our choice for examples brackets this value.

$$\frac{P_{drop}}{area\ of\ drop} = \frac{P}{A} \times \frac{2nd_d}{3\pi d_j} \text{ where } p=nd_j \tag{55}$$

for $d_d = 2 \times d_j$ and $p=4d_j$

$$\frac{P_{drop}}{area\ of\ drop} = \frac{P}{A} \times \frac{16}{\pi} = 6.485 \times \frac{16}{3\pi} \sin\theta \frac{MW}{m^2} \tag{56}$$

At $\theta=22°$ this becomes $4.12\, MW/m^2$.

Using the power per unit area spread over the droplet, we can calculate the evaporation from each droplet as it passes through the divertor. The area of a droplet as a fraction of the divertor area is:

$\frac{area\ of\ drop}{area\ of\ divertor} = \frac{4\pi \frac{d_d^2}{4}}{L \times p} = \frac{3\pi}{8}\frac{d_d}{p} = 0.589$ for our example. Only half of the evaporation moves towards the plasma. So the evaporation per unit area of the divertor is the calculated value per unit area of the droplet times 0.5×0.589.

$J_{drop}=3.28 \times 10^{23}/m^2s$ for flibe and $1.77 \times 10^{20}/m^2s$ for SnLi.

$J_{div\ surface}$=0.5×0.589×3.27x10^{23}/m^{2}s=0.96×10^{23}/m^{2}s

These results are plotted in Fig. 21 as circles for various values of p and n. We can see that droplets will result in more evaporation than jets unless we can make droplets sufficiently small compared to the jet that they are made from (d_d<2d_j). Droplets as with jets must be closely spaced to keep the evaporation less than that of a slab.

A major conclusion of this study is that both jets and droplets can have less evaporation than an equivalent moving slab but with relaxed spacing between jets and droplets the evaporation can become much larger than a slab. A big advantage of jets is the speed can be made very large. We can expect a slab will quickly develop ripples and break up. This will also happen with jets. However, with droplets breakup has already happened and droplets are stable. There are many industrial applications of jets producing droplets: ink jet printers, diesel injectors, flow cytometry.

Multiple-layer analysis–droplets

When is multiple-layer analysis required? As mentioned previously it is when $\theta \le \sin^{-1}\frac{d_d}{L}$

$$L = \frac{2d_d^3}{3d_j^2} \tag{57}$$

$$\theta \le \sin^{-1}\frac{3d_j^2}{2d_d^2}$$

for d_d=2d_j $\theta \le \sin^{-1}\frac{3}{8} = 22^o$ for d_d=1.5d_j $\theta \le \sin^{-1}\frac{2}{3} = 42^o$

Our examples using θ=30° just straddles the need for multiple layer analysis.

The fraction of power incident that is absorbed on the first layer is

$$F = \frac{d_d}{L\sin\theta} = \frac{d_d\, 3d_j^2}{2d_d^3\ \sin\theta} = \frac{3d_j^2}{2d_d^2\ \sin\theta} \tag{58}$$

For $d_d = 2d_j$, $F = \dfrac{3}{8\sin\theta}$ for $\theta > 22^o$ and F=1 for $\theta < 22^o$

For $d_d = 1.5d_j$, $F = \dfrac{2}{3\sin\theta}$ for $\theta > 42^o$ and F=1 for $\theta < 42^o$

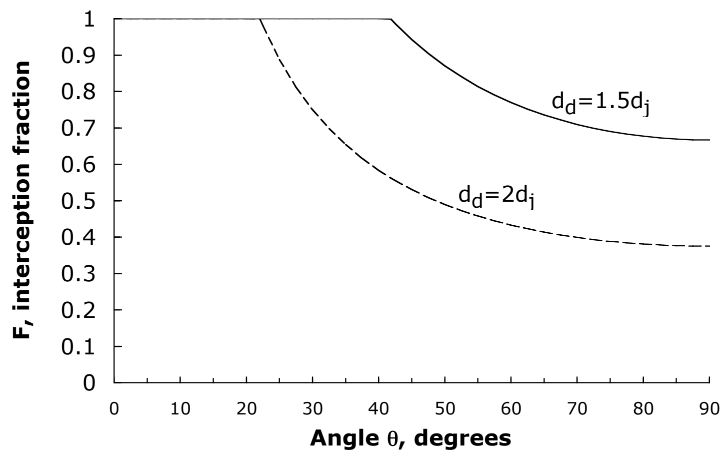

Fig. 23. Fraction of power intercepted on one layer versus angel θ.

From previous experience we find that, when multiple layer analysis is necessary, we are in a regime where the evaporation is high and a better strategy might be to go for closer packed jets and droplet arrays although a multiple-layer arrangement will help high reduce evaporation rates.

The next case we would like to treat is the case of droplets as shown in Fig. 4, 5 and 6. The droplets of adjacent jets are so precisely formed and spaced that we can assume each droplet substantially shields or shadows other droplets, thereby spreading out the power over a large area of multiple droplets as shown in Fig. 4. One layer of droplets might not intercept all the power so we require multiple layers as shown in Fig 4, 5, 6, 24 and **25**.

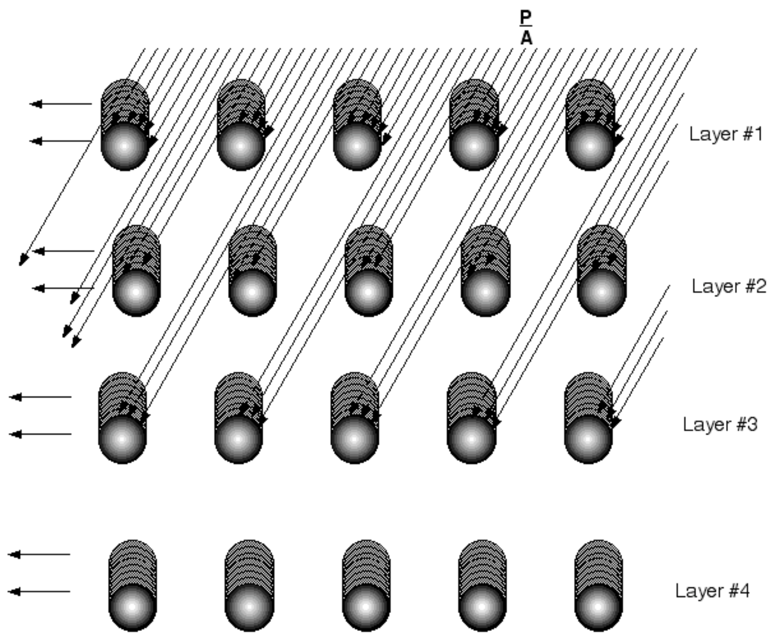

Fig. 24. More than one layer might be needed to intercept all the power (see also Fig. 6).

The incident power gets shadowed on interior layers. We assume the power gets smoothly spread over the surface of the droplet due to spinning and/or the Marangoni convective effect. No credit is taken for convection into the interior by the Marangoni effect although this is expected to be beneficial as discussed earlier. Spinning seems reasonable for molten salt. For liquid metal, MHD effects will produce their own motion but prevent spinning.

For this case, $\theta = 30°$, $\phi = 5.14°$, $\psi = 2.58°$ and $\omega = 90°$. The path length across the diverter is 0.25 m and the average power is 6.485 $\sin\theta$ MW/m^2 assumed to be uniform for our calculation. However, the power onto the row of drops is $72\frac{MW}{m^2}\sin\phi$ and is independent of θ.

The power onto each drop is:

$$P_{drop} = \frac{P}{A} \times p \times d_d \tag{59}$$

$$\frac{P_{drop}}{area\ of\ drop} = \frac{P}{A} \times \frac{p\, d_d}{4\pi \frac{d_d^2}{4}} = 72 \frac{MW}{m^2} \sin\phi \times \frac{p}{\pi\, d_d} \tag{60}$$

The nozzle spacing p in a manifold might be $p=2d_d=4d_j$.

$$\frac{P_{drop}}{area\ of\ drop} = \frac{P}{A} \times \frac{p}{\pi\, d_d} = \frac{2}{\pi} 72 \frac{MW}{m^2} \sin\phi = 4.11\ MW/m^2 \text{ for layer \#1}$$

Note that the power onto the droplet is independent of θ.

For layer #2 we can arrange for shadowing to reduce this power density, for example, by a factor of 2 on each successive row. The spacing between rows, which we have only a little control over is $L = \frac{2d_d^3}{\pi\, d_j^2}$. Each layer can be offset so as to cut the power in half for example. This will require 4 layers to intercept all the power as shown in Fig. 25 for θ=90°.

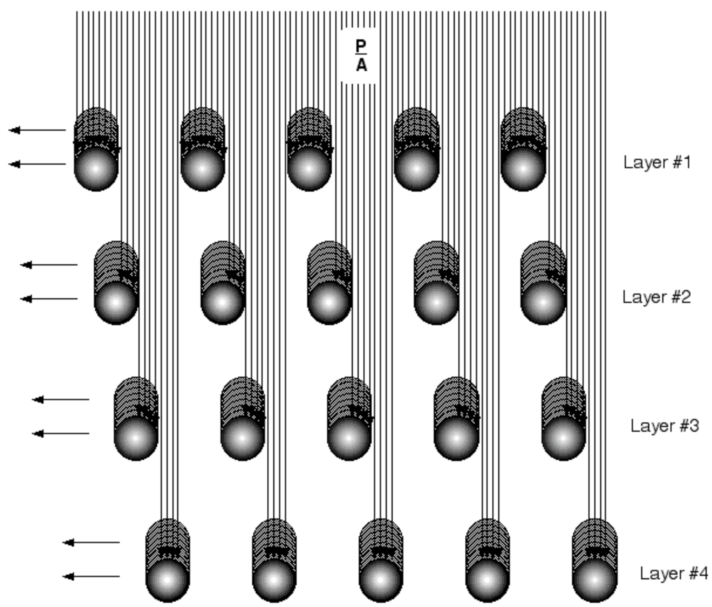

Fig. 25. The droplets are moving to the left across the diverter plasma that is depositing power onto the droplets (θ=90°).

Using the power per unit area spread over the droplet, we can calculate the evaporation from each droplet as it passes through the divertor. The area of a droplet as a fraction of the divertor area is:

$$\frac{area\ of\ \ drop}{area\ of\ \ divertor} = \frac{4\pi \frac{d_d^2}{4}}{L \times p} = \frac{3\pi}{8}\frac{d_d}{p} = 0.589$$ for our example.

The area for condensation or interception of evaporation by each row is:

$$\frac{\text{interception area of drop}}{\text{area of diverter}} = \frac{\pi\, d_d^2/4}{L \times p} = \frac{3\pi}{32}\frac{d_d}{p} = 0.147$$ for our example. The factor of 1/2 comes from half the evaporation heading away from the plasma where it will be condensed. The total evaporation entering the divertor per unit area of the divertor is found by multiplying the evaporation from a droplet times f.

$$f = \frac{1}{2}\frac{3\pi\, d_d}{8p} \times \left(1 - \frac{3\pi\, d_d}{32p}\right)^{n-1} \tag{61}$$

The results of this example are summarized in Table 6 for $p=2d_d$.

Table 4

Evaporation from multiple rows of droplets for $p=2d_d$ and $\theta=90°$ and v=10 m/s.

			Flibe		SnLi	
Row#, n	P/A, MW/m^2	$1/2 \times 0.589\ (1-.147)^{n-1}$	J_{drop}, $10^{21}/m^2s$	J_{net}	J_{drop}, $10^{19}/m^2s$	J_{net}
1	4.11	0.2945	5.58	1.643	3.81	1.122
2	2.055	0.2512	0.283	0.071	1.59	0.399
3	2.055	0.2142	0.283	0.061	1.59	0.341
4	2.74	0.1827	0.813	0.149	2.08	0.380
Total				1.924		2.242

We can compare these results to the slab case with 6.485 $\sin\theta$ MW/m^2 shown in Fig.17 where for 30° we get for flibe $J_{ave}=1.0\times10^{22}/m^2s/\sin\theta=2.0\times10^{22}/m^2s$ and

$4.67\times10^{19}/m^2s/\sin\theta=9.36\times10^{19}/m^2s$ for SnLi. The flibe multi-layer analysis gets 47 times less evaporative flux and the SnLi gives 4.2 times less evaporative flux.

We now show the effect of increasing the power density for a case with two times the power.

Table 7

Evaporation from multiple rows of droplets for $p=2d_d$ and $\theta=90°$ and v=10 m/s and 12.97 MW/m^2.

			Flibe		SnLi	
Row#, n	P/A, MW/m^2	1/2x0.589 $(1-.147)^{n-1}$	J_{drop}, $10^{21}/m^2s$	J_{net}	J_{drop}, $10^{19}/m^2s$	J_{net}
1	8.22	0.2945	491	144.6	21.2	1.122
2	4.11	0.2512	5.583	1.4	3.82	0.96
3	4.11	0.2142	5.583	1.20	3.82	0.82
4	5.48	0.1827	30.22	5.52	6.82	1.25
Total				152.7		4.15

The droplets have an advantage over a slab at the same speed of liquid and by going to higher speed on can get lots more power handling.

Evaporative flux limited by Brook's sheath collapse criterion

Brooks and Naujoks (BROOKS AND NAUJOKS, 2000 and NAUJOKS AND BROOKS, 2001) defined a quantity G=particle refluxing from the diverter across the divertor sheath plasma/particle influx from the edge plasma. When G>1 the sheath can collapse owing to plummeting electron temperature and when G<1 the sheath is stable. For our example with a double null divertor with an average heat flux $6.485\sin\theta$, the average particle flux is $7.5\times10^{23}\sin\theta/m^2s$ averaged over the 0.25 m× $\sin\theta$ divertor plate (Rognlien, 2008 quotes $6.75\times10^{23}/m^2s$ for θ=30° averaged over a distance of 0.14 m).

The slab example at a speed of 10 m/s got $J_{ave}=1\times10^{22}/m^2s$ at θ=30° for 6.485 sinθ MW/m^2 when referred to 90° $J_{ave}=2\times10^{22}/m^2s$. Then

$G=2\times10^{22}/m^2s/7.5x10^{23}\sin\theta/m^2s=0.03$ at θ=90°. (62)

Apparently the sheath is stable for flibe. The SnLi evaporative flux is much less.

The G value for the droplet injection at 10 m/s is $1.792 \times 10^{21}/m^2s/7.5\times10^{23}\sin\theta/m^2s=0.0048$ for θ=90° for flibe. The results seem to show more than adequate heat removal ability especially with droplets.

We can expect higher power handling. For example, at double the power or 13 sinθ MW/m^2 the evaporative flux at 4 x 10 m/s is the same $1\times10^{22}/m^2s$ for the slab and $1.792 \times 10^{21}/m^2s$ for the droplet case. At 10 m/s $G=1.53\times10^{23}/m^2s/7.5x10^{23}=0.2$ for flibe. At 40 m/s G=0.2 for 26 MW/m^2sinθ. Apparently quite high power density can be handled with a droplet divertor.

Divertor design/nozzle design

In this section the design of the nozzles that produce the droplet jets is discussed. The two divertor plates shown in Fig. 1 and 2 are replaced with droplet forming jet arrays as shown in Fig. 26. The power flow across the separatrix on the inboard side (left in Fig 26) is much less than on the outboard side and therefore is less demanding. We will henceforth only discuss the outboard jet set that is shown in more detail in Fig. 27.

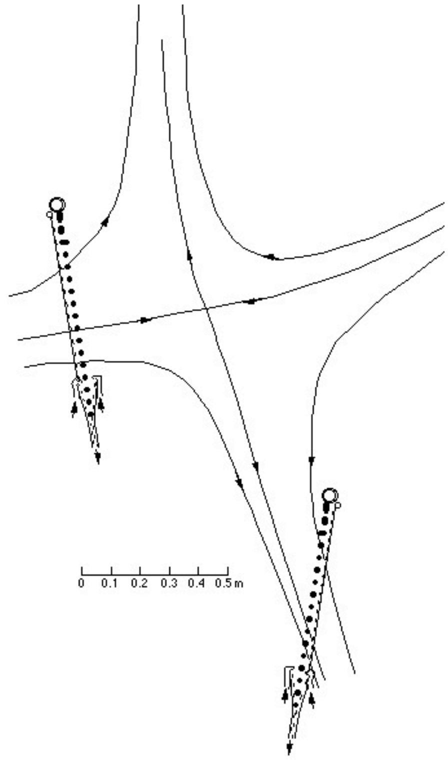

Fig. 26. Divertors are shown made of arrays of droplets.

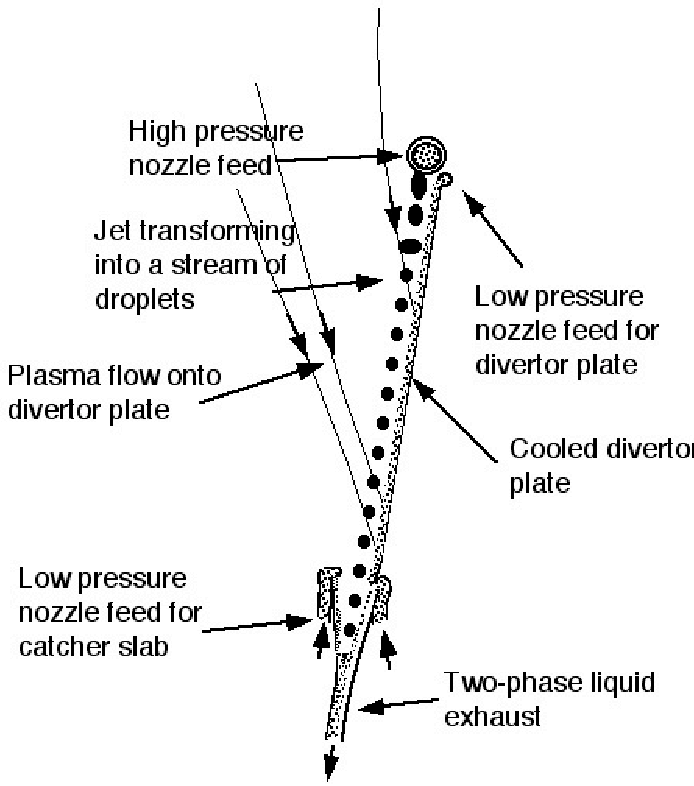

Fig. 27. Details of the droplet divertor.

A high-pressure manifold supplies pressurized liquid to the nozzles. A jet is formed that pinches off into precisely sized droplets aided by an acoustic transducer (not shown). The high-speed droplets are directed into a tapered catcher too avoid erosion by high-speed droplets impacting the surface. Slow moving slab jets are produced to protect the wall from erosion. Grazing incidence impact at small enough angle should minimize or eliminate back splash. In addition some pumping of gases can be expected by gas entrainment into the exiting two-phase gas-liquid flow.

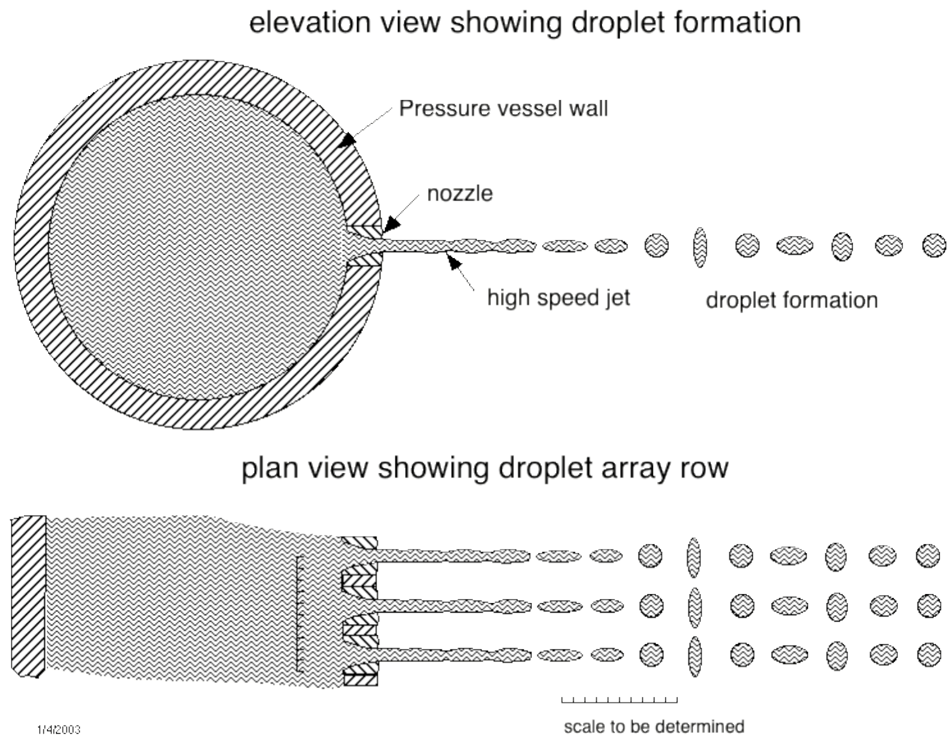

Fig. 28. A pressure transducer (not shown) aids making precise droplets that can be coherent and therefore self-shielding.

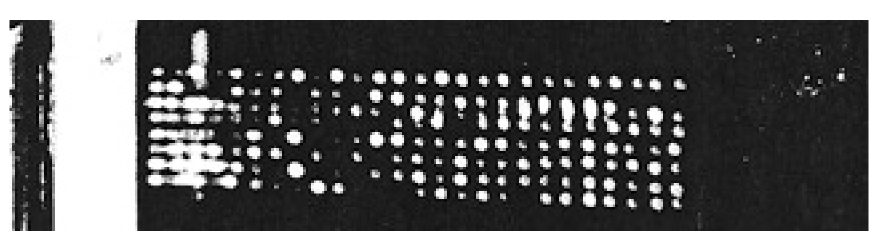

Fig. 29. Ga droplets are shown well aligned based on (Mirnov, Dem'yanenko, and Murav'ev, 1992).

The droplets shown in Fig. 29 are coherent from one jet to the next. This allows droplets from one jet to shadow the ones from adjacent jets.

Spatial coherence condition

The condition for the droplets to be coherent spatially from one jet to the next will depend on their velocity of the jet and angular dispersion of the jet making the droplets. The spatial variation in the direction of travel of the droplet is $\Delta\ell = \frac{\Delta v\, \ell}{v}$. For good coherence we might require the $\Delta\ell < 0.1 d_d = 0.1\times 0.001 m = 10^{-4}\ m$ in a distance of passage across the divertor of 0.3 m of 1 mm diameter droplets of speed 40 m/s. The variation in speed of the jet that produced the droplets could only vary from one to the next by $\frac{\Delta v}{v} = \frac{\Delta\ell}{\ell} = \frac{10^{-4}\ m}{0.3 m} = 3.3\times 10^{-4}$. This requirement does not seem too severe to meet.

The angular dispersion of the jet to keep the droplet location transversely only 0.1 diameter is
$\frac{0.1 d_d}{\ell} = \frac{0.1\times 0.001 m}{0.3 m} = \pm 3.3\times 10^{-4}\ radians = 0.019\,\text{degrees}$. Experimental work will be needed to see if these spatially coherent conditions can be satisfied.

The plasma striking the droplets and the evaporative flux both will have the effect of “pushing” droplets and those “sticking out” more will be pushed back more. This effect that is more important as the droplet size is reduced and for slower speeds will tend to self correct somewhat for droplet lack of coherence owing to a small dispersion in the jets making them.

Acoustic frequency to make droplets

Liquid jets can be used, however, they are unstable to breaking into droplets. The droplets can be made to be almost exactly alike. By oscillating the speed v of the jet as it exits its nozzle by for example driving a pressure transducer at a frequency f, we can superimpose a small perturbation on the jet. This will cause the sausage pinch instability driven by surface tension to squeeze off the jet into precise droplets whose spacing L and radius r_d is repeated to a high precision. For jet radius r_j half the size of the droplet radius r_d, we get $L=16r_d/3$.

$$f = \frac{v}{L} \tag{63}$$

$$f = \frac{3v}{16r_d} \tag{64}$$

$f = \dfrac{3 \times 10\, m/s}{16 \times 0.4 \times 10^{-3}\, m}$ = 4.8 kHz for 0.4 mm radius droplets at 10 m/s (48 kHz at 100 m/s.

Power to make jets

From Bernouli's equation the pressure inside the manifold is P

$$P = \tfrac{1}{2}\rho v^2 + \sigma \frac{\pi d_j}{\pi d_j^2/4} + viscous\ term \tag{65}$$

The pumping power for a single jet is

$$P_{jet} = (\tfrac{1}{2}\rho v^2 + \sigma \frac{\pi d_j}{\pi d_j^2/4} + viscous\ term)\pi d_j^2 v/4 \tag{66}$$

$$P_{jet} = \tfrac{1}{8}\pi d_j^2 \rho v^3 + \sigma \pi d_j v + viscous\ term \times \pi d_j^2 v/4 \tag{67}$$

The first term gives the kinetic power in the jet, the second term is the power going into overcoming surface tension (and at 10 m/s is 100 times less than the first term) and the third term is the dissipation in viscous effects.

The number of jets in a single layer is $\frac{2\pi 4.3m}{p}$. For the case of 1 mm diameter jets and pitch p = $4d_j$=4x0.001 m=0.004 m. Then 6750 jets would be needed for one layer. The pumping power for flibe is 53 kW at 10 m/s and is proportional to v^3. At 100 m/s the power is 53 MW. The manifold pressure is 1 atmos at 10 m/s and 100 atmos at 100 m/s. For SnLi the power and pressure is three times more for the same size and speed. Since the evaporation is so much less for SnLi slower speeds can be used to compensate for the higher pumping power. For 1/2 mm dia jets the pumping power is eight times less.

Suggested future study

The study at this point has shown the advantage of use of droplets. The circulation speed is estimated, however, it remains to be shown by more study if the circulation rate or time is fast enough to distribute the incident heat flux over the whole surface area of a sphere. In additions a number of specific items for further research are recommended:

1-Put in time dependent heat flux in calculations to account for the varying power across the divertor.

2-Include properties varying with temperature in the heat transfer processes. This might decreased the predicted evaporative flux.

3-Put in condensation correction to the evaporation processs. This effect should decreased the predicted evaporative flux.

4-Put in evaporative cooling and other corrections to the evaporation process. This effect should also decreased the predicted evaporative flux.

5-Compute surface temperature on a convecting droplet versus time. This will tell us how much confidence to have in our assumption of spreading the heat flux over the entire droplet surface.

Conclusions

Apparently and surprisingly, jets can have less evaporative flux than a slab by more than an order of magnitude if the spacing is properly chosen. If the spacing between jets is larger than about 4 jet diameters the evaporative flux is larger than for a moving slab. Droplets can have a further reduction in evaporative flux. By employing multiple layers of droplets a large further reduction in net evaporative flux is obtained. At 40 m/s speed flibe droplets can handle a heat flux on the divertor of 25 MW/m^2 normal to the poloidal flow and keep the evaporative flux below the Brook's sheath collapse condition. Liquid metals can handle even higher heat fluxes, however, use of molten salt relieves the worry of MHD effects. Should liquid walls made of flibe turn out to be feasible then the same liquid as a divertor looks feasible whereas liquid metal walls have much more severe problems in a magnetic field.

Acknowledgements

Help from Ed Morse and Dick Bulmer are appreciated. Discussions with Tom Rognlien are acknowledged. Advice on references by Prof. S. Sadhal is appreciated. Support by Vallecitos Molten Salt Research and Kyoto University, Institute of Advanced Energy is appreciated.

References

R. Bulmer (October, 2001), Private communications.

J. N. BROOKS AND D. NAUJOKS, (2000), "Sheath superheat transmission due to redeposition of thermally emitted material," *Phys. Plasmas,* **7,** 2565.

D. NAUJOKS AND J.N. BROOKS, (2001), "Combined sheath and thermal analysis of overheated surfaces in fusion devices," *J. Nucl. Mater.,* **290-293,** 1123.

H. S. Carslaw and J. C. Jaeger, (1958), Conduction of heat in solids, Second Edition, Clarendon Press, Oxford, p242.

Volker Kachel (1990), Chapt 3, pg 27-44, "Hydrodynamic Properties of Flow Cytometry Instruments" in the book "Flow Cytometry and Sorting", 2nd edition, by Melamed, Lindmo, and Mendelsohn, Wiley Liss.

A. A. Karashaev, S. N. Zadumkin and A. I. Kukhno, Zh. Fiz. Khim, **41** (1967) 654, English translation in: Russian Journal of Physical Chemistry, **41** (3), 329-330 (1967).

H. Lamb (1945), Hydrodynamics, Sixth Edition New York, Dover Publications, p 245.

M. A. Mahdavi and M. Schaffer (1998), "Scrape Off Layer Plasma Behavior in Presence of Open Liquid Metal Surfaces," General Atomics unpublished report.

S. V. Mirnov, V. N. Dem'yanenko, and E. V. Murav'ev, "Liquid-metal tokamak divertors," J. Nucl. Mat. **196-198,** 45-49 (1992).

S. V. Mirnov, Private communications, Ga droplets in T-3M (May, 2002).

R.W. Moir, R.H. Bulmer, T.K. Fowler, T.D. Rognlien, M.Z. Youssef, "Thick liquid-walled spheromak magnetic fusion power plant," LLNL Report UCRL-ID-148021 (2002). R.W. MOIR, R.H. BULMER, T.K. FOWLER, T.D. ROGNLIEN, M.Z. YOUSSEF, "Spheromak magnetic fusion power plant with thick liquid-walls," *Fusion Science and Technology,* **44,** 317-326 (2003).

R. W. Moir, R. H. Bulmer, K. Gulec, P. Fogarty, B. Nelson, M. Ohnishi, M. Rensink, T. D. Rognlien, J. F. Santarius, and D. K. Sze, "Thick liquid-walled, field-reversed configuration-magnetic fusion power plant," Fusion Technology 39 (2001) 758-767.

R. W. Moir and T. D. Rognlien (2007), "Axisymmetric tandem mirror magnetic fusion energy power plant with thick liquid-walls," *Fusion Science and Technology* **52**, 408-416.

E. Morse (October 2001), Private communications.

D. R. OLANDER, G. T. FUKUDA, and C. F. BAES, JR., "Equilibrium pressure over BeF_2/LiF (Flibe) molten mixtures," *Fusion Technology*, **41,** 141 (2002).

D. L. R. Oliver and K. J. DeWitt, (1988) "Surface tension driven flows for a droplet in a micro-gravity environment," Int. J. Heat Mass Transfer, 31 1534-1537.

R. D. Rognlien and M. E. Rensink (2002), "Edge-plasma models and characteristics for magnetic fusion energy devices," *Nuclear Engineering and Design* **60** 497-514.

T. D. Rognlien, (2008), based on the case in Rognlien and Rensink (2002), private communication, January 29, 2008.

S. S. Sadhal, E. H. Trinh, and P. Wagner, (1992) "Unsteady spot heating of a drop in a microgravity environment, " *Fluid Mechanics Phenomena in Microgravity*, **AMD-154** ASME 105-110.

S. S. Sadhal, P. S. Ayyaswamy and J. N. Chung, Transport Phenomena with Drops and Bubbles, Springer, New York, (1996).

V. Schrock, private communication April 8, 1998.

M. Tillack (November 15, 2001), private communication.

M. Ulrickson, APEX notes from meeting 2000.

K. Yoshikawa, "A continuous high power beam dump of the hot-dog-cooker type," Lawrence Berkeley Laboratory report, LBL-10643 (1980).

M. R. ZAGHLOUL, D, K. SZE and A. R. RAFFRAY, "Thermo-physical properties and equilibrium vapor-composition of lithium fluoride-beryllium fluoride ($2LiF/BeF_2$) molten salt," *Fusion Science and Technology,* **44,** 344-350 (2003).

X. Zhou and M. S. Tillack (1998) "Assessment of Liquid Metal as the Divertor Surface of a Fusion Power Plant," UCSD report UCSD-ENG-079.

X. Zhou, University of Alaska, Fairbanks, private communications November, 2001.

K. Yajima, H. Moriyama, J. Oishi, and Y. Tominaga, "Surface tension of lithium fluoride and beryllium fluoride binary melt," J. Physical Chemistry, **86,** 4193-4196 (1982).